Heliyon 8 (2022) e11720

Contents lists available at ScienceDirect

Heliyon

journal homepage: www.cell.com/heliyon

Research article

A mathematical model analysis of the human melioidosis transmission dynamics with an asymptomatic case

Habtamu Ayalew Engida [a,*], David Mwangi Theuri [b], Duncan Gathungu [b], John Gachohi [c], Haileyesus Tessema Alemneh [d]

[a] Pan African University for Basic Science, Technology and Invocation (PAUSTI)/JKUAT, Nairobi, Kenya
[b] Department of Mathematics, Jomo Kenyatta University of Agriculture and Technology, Nairobi, Kenya
[c] School of Public Health, Jomo Kenyatta University of Agriculture and Technology, Nairobi, Kenya
[d] Department of Applied Mathematics, University of Gondar, Ethiopia

ARTICLE INFO

Keywords:
Melioidosis
Burkholderia pseudomallei
Asymptomatic
Equilibria and stability
Basic reproduction number
Sensitivity analysis
Numerical simulation

ABSTRACT

In this paper, we develop and examine a mathematical model of human melioidosis transmission with asymptomatic cases to describe the dynamics of the epidemic. The basic reproduction number (R_0) of the model is obtained. Disease-free equilibrium of the model is proven to be globally asymptotically stable when R_0 is less than the unity, while the endemic equilibrium of the model is shown to be locally asymptotically stable if R_0 is greater than unity. Sensitivity analysis is performed to illustrate the effect of the model parameters influencing on the disease dynamics. Furthermore, numerical experiments of the model are conducted to validate the theoretical findings.

1. Introduction

Melioidosis is a tropical infectious disease caused by an aerobic, gram-negative bacterium called *Burkholderia pseudomallei* (Ross et al., 2018; Mahikul et al., 2019; Saechan et al., 2022). It is reported mostly known as endemic, with a high number of cases and rate of mortality in numerous nations of the world including Thailand, Singapore, Malaysia, India, Bangladesh and China (Currie and Kaestli, 2016; Luangasanatip et al., 2019; Chowdhury et al., 2022). A recent report suggests that *Burkholderia pseudomallei* causes an estimated 165,000 human infections and 89,000 (54%) deaths annually all over the world (Limmathurotsakul et al., 2016; Wiersinga et al., 2018; Sullivan et al., 2020). *B. pseudomallei* is mainly found in contaminated environments (soil or water) (Currie and Kaestli, 2016; Luangasanatip et al., 2019). Infection commonly occurs by ingestion, percutaneous inoculation and inhalation of the organism from a contaminated environment (Luangasanatip et al., 2019; Chowdhury et al., 2022). Although human-to-human transmission is rare, it has been documented through contact with reproductive fluid, blood or other body fluids of an infected person (Benoit et al., 2015; Singh and Mahmood, 2017). Transmissions from humans to animals and vice versa are extremely uncommon and both animals and humans are susceptible to the *B. pseudomallei* (Currie, 2015; Phillips et al., 2016; Mahikul et al., 2019). However, we do not incorporate zoonotic infection of humans in this work.

Melioidosis is a serious infection in humans and it can be presented in a variety of clinical forms, septicemia, asymptomatic infections, localized with/without septicemia, visceral abscesses and can involve any organ (Benoit et al., 2015; Karunarathna et al., 2018; Chakravorty and Heath, 2019). Currently, there is no vaccine available for the disease (Mahikul et al., 2019; Terefe and Kassa, 2020). Arise up from the clinical manifestation of the melioidosis, a two-phases therapy for the treatment of the *B. pseudomallei* is recommended. An intensive phase of intravenous antibiotics including ceftazidime (CAZ), imipenem, or meropenem for a minimum of 10-14 days, followed by an eradication phase to prolonged oral trimethoprim-sulfamethoxazole (TMP-SMX) drug for 3-6 months (Ross et al., 2018; Mahikul et al., 2019; Fen et al., 2021). However, recent studies reported that *B. pseudomallei* is intrinsically susceptible to several classes of antimicrobial agents that are recommended for treatment of the disease including newer β-lactam antibiotics, especially to all intravenous antibiotics (Phillips et al., 2016; Dutta et al., 2017; Sengyee et al., 2017; Fen et al., 2021).

* Corresponding author.
E-mail address: hayalew21@gmail.com (H.A. Engida).

https://doi.org/10.1016/j.heliyon.2022.e11720
Received 21 March 2022; Received in revised form 26 May 2022; Accepted 11 November 2022

Further, the epidemiology, clinical manifestations and risk factors of the disease are studied in (Tauran et al., 2015; Limmathurotsakul et al., 2016; Currie and Kaestli, 2016; Hinjoy et al., 2018; Wiersinga et al., 2018; Chakravorty and Heath, 2019).

A mathematical model is an essential tool for understanding and explaining the transmission dynamics of disease by using mathematical language. The model helps in forecasting the consequences of diseases in the populations, elucidating crucial aspects of the disease transmission process, recommending effective control and preventative interventions and providing an assessment of the severity and possible scope of the diseases (Li, 2018; Libotte et al., 2020). Some compartmental models have been proposed to address the dynamics of melioidosis transmission from different perspectives. The authors in (Mahikul et al., 2019) studied a susceptible-exposed-infected-recovered-susceptible (SEIRS) model with an asymptomatic class to predict the burden and future trends of the disease incidence in Thailand taking into account population dynamics, seasonal movements, and incidence of diabetes in the human population. In their model the total population is subgrouped into eight classes namely, the susceptible, exposed, asymptomatic infected, symptomatic infected, recovered, diabetic susceptible, severe, and treatment. The authors determined key factors of the disease incidence patterns. The researchers in (Tavaen and Viriyapong, 2019) proposed a susceptible-latently infected-infectious-recovered (SEIR) model for melioidosis transmission by incorporating control factors such as hygiene care and treatment. The results of their work show that both hygiene care and treatment controls should be encouraged to reduce the spread of the disease. An SEIR model for the transmission dynamics of melioidosis is formulated and analyzed in (Terefe and Kassa, 2020). They were incorporated two recrudescence cases of the disease such as relapse and reinfection of individuals from the recovered class in their model.

Motivated by the literature mentioned above, we aim to propose and analyze a compartmental model for the dynamics of melioidosis transmission with an asymptomatic class. We also considered temporary immunity for recovered class in the disease transmission process. The remaining sections of the paper are structured as follows: we present the formulation of the model in Section 2. The qualitative properties of the model solutions, the basic reproduction number and the stability analysis of the steady states are given in Section 3. The sensitivity analysis of the model parameters is performed in Section 4. The numerical results are carried out in Section 5. The concluding results are provided in Section 6.

2. Model formulation

We formulate a compartmental model that describes the dynamic behavior of melioidosis. The model includes two population groups: the human population (host population) and the bacterial (pathogenic) population. The total human population at time t represented by $N(t)$, is subdivided into five distinct classes; susceptible individuals ($S(t)$), latently-infected individuals ($E(t)$), infectious individuals without symptoms ($A(t)$), infectious individuals that are showing symptoms ($I(t)$), and recovered individuals ($R(t)$). Mathematically, the total human population is described as:

$$N(t) = S(t) + E(t) + A(t) + I(t) + R(t). \tag{1}$$

In the formulation of the model, the following assumptions are made:

(i) The new entry for the susceptible human population may be newborns or immigrants at a constant rate of Π.
(ii) The susceptible humans acquire infection of melioidosis through either percutaneous inoculation, inhalation and ingestion of the pathogen from the contaminated environments (soil or water) or direct contact with infectious (asymptomatic and symptomatic) individuals, and negligible transmission from infected animals.
(iii) The incidence from the environment to humans is assumed to be modeled logistically (saturating), and assumed homogeneous mixing for human to human interaction.
(iv) The symptomatic infectious are greater in number than asymptomatic infectious.

The probability of contact between susceptible humans and contaminated environment is represented by $\lambda_1(B_m) = \frac{B_m}{\mathbf{C}+B_m}$, which is a nonlinear function in B_m. The constant $\mathbf{C}$ is the pathogen concentration that yields 50% chance of catching melioidosis. Thus, the number of contact between the environment and susceptible humans is given by $\lambda_1(B_m)S$. Therefore, the number of infections per unit time due to the environment is given by $\beta_1\lambda_1(B_m)S$, where β_1 is the transmission rate due to the environment-to-susceptible human interaction. Whereas, the number of infections per unit time due the infectious individuals (asymptomatic and symptomatic) is given by $\beta_2(I+\sigma A)S$, where β_2 is the transmission coefficient of the disease due to human-to-human interaction and σ is the reduction in infectivity of A with, $0<\sigma<1$. Therefore, the number of susceptible humans infected by the disease per unit time given by λS and join E, where $\lambda = \beta_1\lambda_1(B_m) + \beta_2(I+\sigma A)$ is the force of infection. The individuals in E progress to I with probability θ, and to the A with probability $(1-\theta)$. B_m increases its size in the contaminated environment by A and I with the shedding rate η. Further, the description of the model parameters is summarized in Table 1. We obtained the following system of differential equations from schematic diagram of the melioidosis model in Fig. 1.

$$\begin{cases} \dfrac{dS}{dt} = \Pi + \alpha R - (\lambda+\mu)S, \\ \dfrac{dE}{dt} = \lambda S - (\rho+\mu)E, \\ \dfrac{dA}{dt} = (1-\theta)\rho E - (\delta+\gamma_1+\mu)A, \\ \dfrac{dI}{dt} = \theta\rho E - (\delta+\gamma_2+\mu)I, \\ \dfrac{dR}{dt} = \gamma_1 A + \gamma_2 I - (\alpha+\mu)R, \\ \dfrac{dB_m}{dt} = \eta(A+I) - \mu_b B_m. \end{cases} \tag{2}$$

Where, $\lambda = \beta_1\frac{B_m}{C+B_m} + \beta_2(I+\sigma A)$.
With the initial conditions:
$S(0) = S_0 \geq 0,\ E(0) = E_0 \geq 0,\ A(0) = A_0 \geq 0,\ I(0) = I_0 \geq 0,\ R(0) = R_0 \geq 0,\ B_m(0) = B_{m,0} \geq 0.$

Table 1. Description of parameters of model.

Parameter	Description
Π	Human recruitment rate.
β_1	Transmission rate among environment and susceptible humans.
β_2	Transmission rate among susceptible and infectious humans.
μ	Natural death rate of individuals.
μ_b	Natural death rate of bacteria.
α	Disease waning immunity.
δ	Disease-induced death rate of A and I.
ρ	Progression rate from latent infected to infectious classes.
γ_1	Recovery rate from asymptomatic infectious.
γ_2	Recovery rate from symptomatic infectious.
η	Rate at which bacteria increase by A and I.

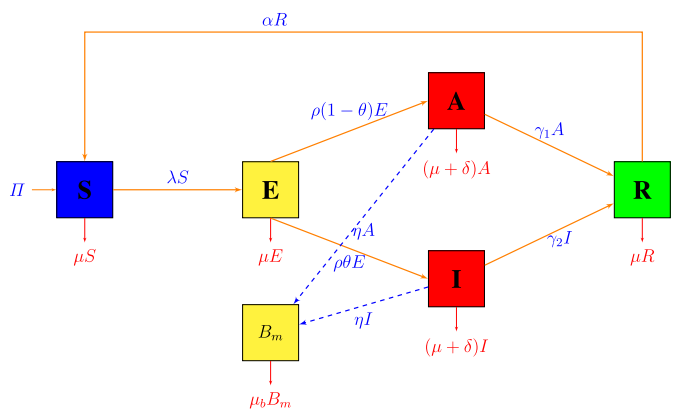

Fig. 1. Schematic diagram for Melioidosis disease dynamics.

3. Model analysis

3.1. Positivity of solutions

For our model (2) to be epidemiologically meaningful, we have established the following nonnegativity result for all of its state variables.

Theorem 3.1. *If $S(0)$, $E(0)$, $A(0)$, $I(0)$, $R(0)$, and $B_m(0)$ are positive initial conditions for the melioidosis model (2), then the solution $\Big(S(t), E(t), A(t), I(t), R(t), B_m(t)\Big)$ of the model (2) is positive for all $t > 0$.*

Proof. Let $t_1 = \sup\Big\{t > 0 : S(t_0), E(t_0), A(t_0), I(t_0), R(t_0),$ and $B_m(t_0)$ are all positive, $\forall t_0$ in $[0, t]\Big\}$. Note that $t_1 > 0$ for non-negative initial conditions. From the first equation of (2), we have

$$\frac{dS}{dt} + (\lambda + \mu)S = \Pi + \alpha R. \tag{3}$$

Now using the variation formula to the equation (3) at $t_1 > 0$, we get

$$S(t_1) = e^{\int_0^{t_1}(-\mu-\lambda)(\tau)d\tau} \times \int_0^{t_1} e^{\int_0^{\tau}(\mu+\lambda)(\tau)d\tau} \times (\Pi + \alpha R)(s)ds + S(0)e^{-\int_0^{t_1}(\mu+\lambda)(\tau)d\tau} > 0.$$

In the same manner, it can be demonstrated that $E(t) > 0$, $A(t) > 0$, $I(t) > 0$, $R(t) > 0$ and $B_m(t) > 0$, $\forall t > 0$. As a result, for all positive initial conditions, all solutions of the model (2) remain positive.

3.2. Invariant region

In this section, we need to establish a biologically feasible region in which the model (2) solution is bounded. The feasible region of the model equation (2) is stated as follows.

Lemma 3.2. *Every solution of the model (2) remains in the closed set, $\Omega_m = \Big\{\big(S, E, A, I, R, B_m\big) \in R_+^6 : 0 \le N(t) \le \frac{\Pi}{\mu}, 0 \le B_m(t) \le \frac{\eta\Pi}{\mu_b\mu}\Big\}$.*

Proof. From the equations (1) and (2), we obtain

$$\frac{dN}{dt} = \Pi - \mu N - \delta(A + I) \le \Pi - \mu N = \mu(\frac{\Pi}{\mu} - N). \tag{4}$$

Note that if $N \leq \frac{\Pi}{\mu}$, then $\frac{dN}{dt} \geq 0$ and $\frac{dN}{dt} < 0$ whenever $N > \frac{\Pi}{\mu}$. Thus, by using the standard comparison theorem in (Lakshmikantham et al., 1989) and variation of formula to the differential inequality (4), we get

$$N(t) \leq N(0)e^{-\mu t} + \frac{\Pi}{\mu}(1 - e^{-\mu t}).$$

It follows that,

$$0 \leq \lim_{t\to\infty} \sup N(t) \leq \frac{\Pi}{\mu}.$$

In particular, if $N(0) \leq \frac{\Pi}{\mu}$, then $N(t) \leq \frac{\Pi}{\mu}$ $\forall t > 0$. Similarly, from the last equation of (2), we found that

$$B_m(t) \leq B_m(0)e^{-\mu_b t} + \frac{\eta\Pi}{\mu_b\mu}(1 - e^{-\mu_b t}) \quad \forall t > 0.$$

This implies that

$$0 \leq \lim_{t\to\infty} \sup B_m(t) \leq \frac{\eta\Pi}{\mu_b\mu}.$$

Therefore, $0 \leq B_m(t) \leq \frac{\eta\Pi}{\mu_b\mu}$ whenever, $0 \leq B_m(0) \leq \frac{\eta\Pi}{\mu_b\mu}$ $\forall t > 0$.

Furthermore, if $N(0) > \frac{\Pi}{\mu}$ ($B_m(0) > \frac{\eta\Pi}{\mu_b\mu}$, respectively), then either the solution enters the region Ω_m in finite time or $N(t) \longrightarrow \frac{\Pi}{\mu}$ ($B_m(t) \longrightarrow \frac{\eta\Pi}{\mu_b\mu}$, respectively) asymptotically as $t \to \infty$. Consequently, the region is positively invariant and attracts all solutions of the system (2) and it suffices to consider the dynamics of the model (2) in Ω_m.

3.3. Disease free equilibrium

The disease-free equilibrium (DFE) point is a point where no disease is present in the population. Since all states are considered to have a constant solution at the equilibrium point, we can then compute DFE by setting the right-hand equations in the system ODE (2) to zero and substituting zero for infective and causative agent classes. Therefore, the DFE point of the system (2) is given by

$$\varepsilon_0^* = \left(S^*, 0, 0, 0, 0, 0\right) = \left(\frac{\Pi}{\mu}, 0, 0, 0, 0, 0\right). \tag{5}$$

3.4. The basic reproductive number and local stability of the DFE

The basic reproduction (or reproductive) number (R_0) is a key concept in epidemiology that provides information on the status of the disease. To derive, R_0, we use the next-generation matrix approach introduced in (Van den Driessche and Watmough, 2002). Based on the method of Van den Driessche and Watmough in (Van den Driessche and Watmough, 2002) the infected compartments of our model are given in the following sub-system:

$$\begin{cases} \frac{dE}{dt} = \lambda S - (\rho + \mu)E, \\ \frac{dA}{dt} = (1-\theta)\rho E - (\delta + \gamma_1 + \mu)A, \\ \frac{dI}{dt} = \theta\rho E - (\delta + \gamma_2 + \mu)I, \\ \frac{dB_m}{dt} = \eta(A + I) - \mu_b B_m. \end{cases} \tag{6}$$

Consider that $F_i(t)$ is the rate of appearance of new infections in compartment i and $V_i(t)$ is the rate of transfer of individuals into and out of compartment i, for, $i = 1, 2, 3, 4$. Thus, the column matrices $F(t)$ and $V(t)$ associated with the system ODE (6), are given by:

$$F(t) = \begin{bmatrix} F_1(t) \\ F_2(t) \\ F_3(t) \\ F_4(t) \end{bmatrix} = \begin{bmatrix} \lambda S \\ 0 \\ 0 \\ 0 \end{bmatrix}, \quad V(t) = \begin{bmatrix} V_1(t) \\ V_2(t) \\ V_3(t) \\ V_4(t) \end{bmatrix} = \begin{bmatrix} (\rho + \mu)E \\ -(1-\theta)\rho E + (\delta + \gamma_1 + \mu)A \\ -\theta\rho E + (\delta + \gamma_2 + \mu)I \\ -\eta(A + I) + \mu_b B_m \end{bmatrix}.$$

Thus, the associated Jacobian matrices of $F(t)$ and $V(t)$ at ε_0^* are found as follows:

$$F = \begin{bmatrix} 0 & \frac{\beta_2\sigma\Pi}{\mu} & \frac{\beta_2\Pi}{\mu} & \frac{\beta_1\Pi}{C\mu} \\ 0 & 0 & 0 & 0 \\ 0 & 0 & 0 & 0 \\ 0 & 0 & 0 & 0 \end{bmatrix} \text{ and } V = \begin{bmatrix} \rho + \mu & 0 & 0 & 0 \\ -(1-\theta)\rho & (\delta + \gamma_1 + \mu) & 0 & 0 \\ -\theta\rho & 0 & (\delta + \gamma_2 + \mu) & 0 \\ 0 & -\eta & -\eta & \mu_b \end{bmatrix}.$$

Now, the next generation matrix of the model (2) is the product of F and V^{-1}. Computing the product FV^{-1}, yields

$$FV^{-1} = \begin{bmatrix} 0 & \frac{\beta_2\sigma\Pi}{\mu} & \frac{\beta_2\Pi}{\mu} & \frac{\beta_1\Pi}{C\mu} \\ 0 & 0 & 0 & 0 \\ 0 & 0 & 0 & 0 \\ 0 & 0 & 0 & 0 \end{bmatrix} \begin{bmatrix} \frac{1}{\rho+\mu} & 0 & 0 & 0 \\ \frac{(1-\theta)\rho}{(\rho+\mu)\epsilon_1} & \frac{1}{\epsilon_1} & 0 & 0 \\ \frac{\theta\rho}{(\rho+\mu)\epsilon_1} & 0 & \frac{1}{\epsilon_2} & 0 \\ \frac{\eta}{\mu_b(\rho+\mu)}\left(\frac{(1-\theta)\rho}{\epsilon_1} + \frac{\theta\rho}{\epsilon_2}\right) & \frac{\eta}{\mu_b\epsilon_1} & \frac{\eta}{\mu_b\epsilon_2} & \frac{1}{\mu_b} \end{bmatrix} = \begin{bmatrix} \alpha_1 & \alpha_2 & \alpha_3 & \alpha_4 \\ 0 & 0 & 0 & 0 \\ 0 & 0 & 0 & 0 \\ 0 & 0 & 0 & 0. \end{bmatrix}$$

Where,

$$\alpha_1 = \frac{\Pi\rho\left[\theta\epsilon_1(C\beta_2\mu_b + \eta\beta_1) + (1-\theta)\epsilon_2(C\beta_2\sigma\mu_b + \eta\beta_1)\right]}{C\mu\mu_b\epsilon_1\epsilon_2(\rho+\mu)}, \quad \alpha_2 = \frac{\Pi(\beta_1\eta + C\beta_2\sigma\mu\mu_b)}{C\mu\mu_b\epsilon_1},$$

$$\alpha_3 = \frac{\Pi(\beta_1\eta + C\beta_2\mu\mu_b^2\epsilon_1)}{C\mu\mu_b^2\epsilon_1\epsilon_2}, \quad \alpha_4 = \frac{\Pi\beta_1}{C\mu\mu_b}, \quad \epsilon_1 = \delta + \gamma_1 + \mu, \quad \epsilon_2 = \delta + \gamma_2 + \mu.$$

Thus, the eigenvalues of the next generation matrix (FV^{-1}) are

$$\lambda_1 = \frac{\Pi\rho\left[\theta\epsilon_1(C\beta_2\mu_b + \eta\beta_1) + (1-\theta)\epsilon_2(C\beta_2\sigma\mu_b + \eta\beta_1)\right]}{C\mu\mu_b\epsilon_1\epsilon_2(\rho+\mu)}, \quad \lambda_2 = \lambda_3 = \lambda_4 = 0.$$

The required basic reproduction number of the model equation (2) is found through the spectral radius of the matrix $R_0 = \rho(FV^{-1}) = \lambda_1$. Hence,

$$R_0 = \Pi\rho\left(\frac{\beta_1\eta(\theta\epsilon_1 + (1-\theta)\varepsilon_2) + C\mu_b\beta_2(\theta\epsilon_1 + \sigma(1-\theta)\varepsilon_2)}{(\rho+\mu)C\mu\mu_b\epsilon_1\epsilon_2}\right) \tag{7}$$

The equation (7) can be written as

$$R_0 = R_{0h} + R_{0b}.$$

Where,

$$R_{0h} = \frac{\Pi\rho\beta_2\left[\theta(\delta+\gamma_1+\mu) + \sigma(1-\theta)(\delta+\gamma_2+\mu)\right]}{\mu(\rho+\mu)(\delta+\gamma_1+\mu)(\delta+\gamma_2+\mu)},$$

is the basic reproduction number due to human-to-human transmission, and

$$R_{0b} = \frac{\Pi\rho\beta_1\left[\theta(\delta+\gamma_1+\mu) + (1-\theta)(\delta+\gamma_2+\mu)\right]}{C\mu\mu_b(\rho+\mu)(\delta+\gamma_1+\mu)(\delta+\gamma_2+\mu)},$$

is the basic reproduction number due to environment-to-human transmission.

Based on the Theorem 2 by (Van den Driessche and Watmough, 2002), we have the following standard result for the local stability of the DFE, ε_0^*.

Theorem 3.3 *(Local stability of the DFE). The DFE, ε_0^*, of the model (2) is locally asymptotically stable if $R_0 < 1$ and unstable if $R_0 > 1$.*

3.5. Global stability of the DFE

We use the method presented in (Castillo-Chavez et al., 2002; Liao and Wang, 2011; Kanyi et al., 2021) to examine the global stability of the DFE of the model (2). We first denote the system (2) by

$$\begin{cases} \dfrac{dX_1}{dt} = G_1(X_1, X_2), \\ \dfrac{dX_2}{dt} = G_2(X_1, X_2), G(X_1, 0) = 0, \end{cases}$$

where $X_1 = (S, R)$ denotes uninfected classes and $X_2 = (E, A, I, B_m)$ represents the infected classes including the bacterial population class. The DFE point of the model, $\varepsilon_0^* = (\frac{\pi}{\mu}, 0, 0, 0, 0, 0)$, is guaranteed to be globally asymptotically stable (GAS) if $R_0 < 1$ (which is locally asymptotically stable) and the following two conditions C_1 and C_2 hold:

C_1: For $\frac{dX_1}{dt} = G_1(X_1, 0)$, if $X_1^* = \left(\frac{\pi}{\mu}, 0\right)$ is GAS, where X_1^* is DFE point of the system $\frac{dX_1}{dt}$.

C_2: $G_2(X_1, X_2) = AX_2 - G_2^\star(X_1, X_2), G_2^\star(X_1, X_2) \geq 0, \forall(X_1, X_2) \in \Omega_m$, where A is an M-matrix which is given by $A = \frac{\partial G_2(X_1^*, 0)}{\partial X_2}$. Note that $(X_1^*, 0) = \varepsilon_0^* = (\frac{\pi}{\mu}, 0, 0, 0, 0, 0)$.

Theorem 3.4. *The DFE, ε_0^*, given by (5), is GAS (2) provided that $R_0 < 1$.*

Proof. We simply need to demonstrate that the criteria C_1 and C_2 are true when $R_0 < 1$. In the system of the model equation (2), we have

$$G_1(X_1, 0) = \begin{bmatrix} \Pi + \alpha R - \mu S \\ -(\alpha+\mu)R \end{bmatrix}, \quad X_1^* = \left(\frac{\pi}{\mu}, 0\right).$$

We note that $R'(t) = -(\alpha+\mu)R$ is linear ODE and its solution can be easily found as

$$R(t) = R_0 e^{-(\alpha+\mu)t}. \tag{8}$$

Also, $S'(t) = \Pi + \alpha R - \mu S$, and equation (8) yields, $S'(t) = \Pi + \alpha R_0 e^{-(\alpha+\mu)t} - \mu S$ and its solution is given by

$$S(t) = \frac{\Pi}{\mu} + S_0 e^{-\mu t} - R_0 e^{-(\alpha+\mu)t}.$$

Now, consider t $\to \infty$, to show $X_1 \to X_1^*$. Clearly, $R(t) \to 0$ and $S(t) \to \frac{\Pi}{\mu}$ as t $\to \infty$, regardless of the values of R_0 and S_0. As a result, all points that satisfy these criteria converge to $X_1^* = (\frac{\pi}{\mu}, 0)$. Hence, $X_1^* = (\frac{\pi}{\mu}, 0)$ is GAS.

Next, consider

$$G_2(X_1,X_2)=\begin{bmatrix} G_{21}(X_1,X_2)\\ G_{22}(X_1,X_2)\\ G_{23}(X_1,X_2)\\ G_{24}(X_1,X_2)\end{bmatrix}=\begin{bmatrix} \beta_1(\frac{B_m}{C+B_m})S+\beta_2(I+\sigma A)S-(\rho+\mu)E\\ (1-\theta)\rho E-(\delta+\gamma_1+\mu)A\\ \theta\rho E-(\delta+\gamma_2+\mu)I\\ \eta(A+I)-\mu_b B_m\end{bmatrix},$$

and $G_2(X_1,X_2)=AX_2-G_2^{\star}(X_1,X_2)$. Where,

$$A=\begin{bmatrix} -(\rho+\mu) & \frac{\beta_2\sigma\Pi}{\mu} & \frac{\beta_2\Pi}{\mu} & \frac{\beta_1\Pi}{C\mu}\\ (1-\theta)\rho & -(\delta+\gamma_1+\mu) & 0 & 0\\ \theta\rho & 0 & -(\delta+\gamma_2+\mu) & 0\\ 0 & \eta & \eta & -\mu_b\end{bmatrix} \text{ and } G_2^{\star}(X_1,X_2)=\begin{bmatrix}\Delta\\0\\0\\0\end{bmatrix},$$

with, $\Delta=\beta_2(I+\sigma A)\left(\frac{\Pi}{\mu}-S\right)+\frac{\beta_1 B_m}{C}\left(\frac{\Pi}{\mu}-\frac{CS}{C+B_m}\right)$.

We have, $0\le\frac{CS}{C+B_m}\le S\le\frac{\Pi}{\mu}$ ($\because\frac{C}{C+B_m}\le 1$ and all parameters are nonnegative). As a result, $\left(\frac{\Pi}{\mu}-S\right)\ge 0$ and $\left(\frac{\Pi}{\mu}-\frac{CS}{C+B_m}\right)\ge 0$. Thus, $G_2^{\star}(X_1,X_2)\ge 0$ $\forall(X_1,X_2)\in\Omega_m$. Therefore, the DFE, $\varepsilon_0^*=(\frac{\pi}{\mu},0,0,0,0,0)$, of the system (2) is GAS.

Remark 1. The model (2) does not show a backward bifurcation at $R_0=1$ when $R_0<1$. According to Theorem 3.4, the only positive (or stable) steady state for $R_0<1$ is DFE. This is because some typical cases of backward bifurcation in epidemic models weren't considered in our model.

The common causes for the existence of backward bifurcation in some standard deterministic models including reinfection have been studied in (Elbasha et al., 2011; Gumel, 2012). For instance, backward bifurcation has been seen in the melioidosis epidemic model (Terefe and Kassa, 2020) due to reinfection and relapse of recovered individuals.

3.6. Endemic equilibrium

An endemic equilibrium (EE) point is a state where the disease remains in the population. By setting the system (2) equal to zero at steady state, the EE point of our model is obtained. Thus,

$$\begin{cases} \frac{dS^*}{dt}=\Pi+\alpha R^*-(\beta_1\frac{B_m^*}{C+B_m^*}+\beta_2(I^*+\sigma A^*)+\mu)S^*=0,\\ \frac{dE^*}{dt}=(\beta_1\frac{B_m^*}{C+B_m^*}+\beta_2(I^*+\sigma A^*))S^*-(\rho+\mu)E^*=0,\\ \frac{dA^*}{dt}=(1-\theta)\rho E^*-(\delta+\gamma_1+\mu)A^*=0,\\ \frac{dI^*}{dt}=\theta\rho E^*-(\delta+\gamma_2+\mu)I^*=0,\\ \frac{dR^*}{dt}=\gamma_1A^*+\gamma_2I^*-(\alpha+\mu)R^*=0,\\ \frac{dB_m^*}{dt}=\eta(A^*+I^*)-\mu_bB_m^*. \end{cases} \tag{9}$$

From the equations in (9), solving the other state variables in terms of I^*, we found the EE of the model (2) as:

$$\begin{aligned}\varepsilon_1^*&=\left(S^*,E^*,A^*,I^*,R^*,B_m^*\right)\\ &=\left(\frac{\Pi+\alpha R^*}{\mu+\lambda^*},\frac{\epsilon_2}{\rho\theta}I^*,\frac{(1-\theta)\epsilon_2}{\theta\epsilon_1}I^*,I^*,\left(\frac{\gamma_1(1-\theta)\epsilon_2+\gamma_2\theta\epsilon_1}{(\alpha+\mu)\theta\epsilon_1}\right)I^*,\left(\frac{\eta(1-\theta)\epsilon_2+\eta\theta\epsilon_1}{\mu_b\theta\epsilon_1}\right)I^*\right).\end{aligned} \tag{10}$$

Where, $\epsilon_1=(\delta+\gamma_1+\mu),\epsilon_2=(\delta+\gamma_2+\mu)$. Then by substituting all the right-hand side expressions in (10) into the second equation of the system (9), we found the following quartic equation for I^*:

$$P_m(I^*)=I^*\left(A(I^*)^3+B(I^*)^2+CI^*+D\right)=0. \tag{11}$$

Where,

$$\begin{aligned} A&=-\beta_2\epsilon_1\theta^2\eta^2\left[\left(\theta\epsilon_1+(1-\theta)\epsilon_2\right)^2\left(\theta\epsilon_1+\sigma(1-\theta)\epsilon_2\right)\right]\left[\alpha\rho(\gamma_1(1-\theta)\epsilon_2+\gamma_2\theta\epsilon_1)-(\rho+\mu)(\alpha+\mu)\epsilon_1\epsilon_2\right],\\ &=-\beta_2\epsilon_1\theta^2\eta^2\left[\left(\theta\epsilon_1+\sigma(1-\theta)\epsilon_2\right)\left((1-\theta)\epsilon_2+\theta\epsilon_1\right)^2\right]\times\Psi_1<0,\\ B&=-\theta^3\epsilon_1^2\eta\left(\theta\epsilon_1+(1-\theta)\epsilon_2\right)\left[\Psi_1\times\Psi_2+\Psi_3\right]<0,\ \text{if } R_0\le 1,\\ C&=-\theta^4\epsilon_1^3\mathbf{C}\mu_b\left(\Psi_1\times\Psi_4+\Psi_5\right)<0,\ \text{if } R_0\le 1,\\ D&=\theta^5\epsilon_1^4(\alpha+\mu)(\rho+\mu)\mathbf{C}^2\mu_b^2\mu\epsilon_1\epsilon_2(R_0-1)>0 \text{ if } R_0>1, \end{aligned}$$

with,

Table 2. Possible positive real roots of $P_m(I_h^*)$ for $R_0 > 1$, $R_0 < 1$ and $R_0 = 1$.

Cases	A	B	C	D	R_0	No. of sign changes	No. of possible positive real roots
1	-	+	+	+	$R_0 > 1$	1	1
2	-	-	-	+	$R_0 > 1$	1	1
3	-	-	+	+	$R_0 > 1$	1	1
4	-	+	-	+	$R_0 > 1$	3	1, 3
5	-	-	-	-	$R_0 < 1$	0	0
6	-	-	-	0 (No sign)	$R_0 = 1$	0	0

$$\begin{cases} \Psi_1 = \alpha\rho\Big(\gamma_1\theta(\delta+\mu)+\gamma_2(1-\theta)(\delta+\mu)+(\delta+\mu)^2\Big)+\mu\epsilon_1\epsilon_2\big(\rho+\alpha+\mu\big), \\ \Psi_2 = \beta_1\eta\big(\theta\epsilon_1+(1-\theta)\epsilon_2\big)+2\beta_2\mathbf{C}\mu_b\big(\theta\epsilon_1+\sigma(1-\theta)\epsilon_2\big), \\ \Psi_3 = \eta(\alpha+\mu)(\theta\epsilon_1+(1-\theta)\epsilon_2)(\rho+\mu)\mu\epsilon_1\epsilon_2(1-R_{0h}), \\ \Psi_4 = \beta_1\eta\big(\theta\epsilon_1+(1-\theta)\epsilon_2\big)+\beta_2\mathbf{C}\mu_b\big(\theta\epsilon_1+\sigma(1-\theta)\epsilon_2\big), \\ \Psi_5 = \eta(\alpha+\mu)(\theta\epsilon_1+(1-\theta)\epsilon_2)(\rho+\mu)\mu\epsilon_1\epsilon_2(1-R_{0h}+1-R_0). \\ \epsilon_1 = (\delta+\gamma_1+\mu), \quad \epsilon_2 = (\delta+\gamma_2+\mu). \end{cases}$$

The zero root of the equation (11) corresponds to the DFE. It is worth noting that the coefficient A is always negative, the coefficients B and C are negative if $R_0 \le 1$, and D is negative or positive if R_0 is less than unity or greater than unity, respectively. Moreover, when $R_0 = 1$, then D is zero (or has no sign) and the equation (11) is reduced to quadratic equation, $A(I^*)^2 + BI^* + C = 0$. So that the quartic equation (11) can be analyzed for the possibility of multiple equilibria. We used the Descartes' rule of signs presented in (Levin, 2020) to analyze the existence of possible positive roots of the polynomial equation (11). This is described in Table 2. Hence, we have established the following result for the existence of the EE.

Theorem 3.5 *(Existence of the EE). The model (2)*
(i) has a unique positive endemic equilibrium if the case (1, 2, or 3) is satisfied,
(ii) has a unique positive endemic equilibrium or three positive endemic equilibria if the case 4 is satisfied,
(iii) has no positive endemic equilibrium if $R_0 \le 1$.

Theorem 3.6 *(Local stability of the EE). The endemic equilibrium,* ε_1^**, of the model (2), described in the equation (14), is locally asymptotically stable for* $R_0 > 1$.

Proof. We use the technique presented in (Castillo-Chavez and Song, 2004), to show the existence of forward bifurcation. The following change for the state variables of the model (2) is performed to implement the procedure. Suppose, $S = x_1$, $E = x_2$, $A = x_3$, $I = x_4$, $R = x_5$, and $B_m = x_6$.

Thus, the vector notation for the variables is given by

$$\mathbf{X} = \big(x_1, x_2, x_3, x_4, x_5, x_6\big)^T. \tag{12}$$

Using the vector notation in (12), the system (2) can be expressed as

$$\frac{dX}{dt} = F(X), \text{ where } F = (f_1, f_2, f_3, f_4, f_5, f_6)^T. \tag{13}$$

Hence, the equation (13) can be rewritten as:

$$\begin{cases} \dfrac{dx_1}{dt} = \Pi + \alpha x_5 - \left(\beta_1\dfrac{x_6}{C+x_6} + \beta_2(x_4+\sigma x_3)+\mu\right)x_1 = f_1, \\ \dfrac{dx_2}{dt} = \left(\beta_1\dfrac{x_6}{C+x_6} + \beta_2(x_4+\sigma x_3)\right)x_1 - (\rho+\mu)x_2 = f_2, \\ \dfrac{dx_3}{dt} = (1-\theta)\rho x_2 - (\delta+\gamma_1+\mu)x_3 = f_3, \\ \dfrac{dx_4}{dt} = \theta\rho x_2 - (\delta+\gamma_2+\mu)x_4 = f_4, \\ \dfrac{dx_5}{dt} = \gamma_1 x_3 + \gamma_2 x_4 - (\alpha+\mu)x_5 = f_5, \\ \dfrac{dx_6}{dt} = \eta(x_3+x_4) - \mu_b x_6 = f_6. \end{cases} \tag{14}$$

Suppose that $\beta_1 = \beta_1^*$ is chosen as bifurcation parameter and computing for β_1^* for $R_0 = 1$, we found that

$$\beta_1^* = \frac{(\rho+\mu)\mathbf{C}\mu\mu_b\epsilon_1\epsilon_2 - C\mu_b\beta_2\Pi\rho(\theta\epsilon_1+\sigma(1-\theta)\epsilon_2)}{\Pi\rho\eta(\theta\epsilon_1+(1-\theta)\epsilon_2)}.$$

Then, the Jacobian matrix of the system of equations (14) computed at $(\epsilon_0^*, \beta_1^*)$ is given by

$$J(\varepsilon_0^*,\beta_1^*)=\begin{bmatrix} -\mu & 0 & -J_1 & -J_2 & \alpha & -J_3 \\ 0 & -J_4 & J_1 & J_2 & 0 & J_3 \\ 0 & J_5 & -J_6 & 0 & 0 & 0 \\ 0 & J_7 & 0 & -J_8 & 0 & 0 \\ 0 & 0 & \gamma_1 & \gamma_2 & -J_9 & 0 \\ 0 & 0 & \eta & \eta & 0 & -\mu_b \end{bmatrix}.$$

Where, $J_1=\frac{\beta_2\sigma\Pi}{\mu}$, $J_2=\frac{\beta_2\Pi}{\mu}$, $J_3=\frac{\beta_1^*\Pi}{C\mu}$, $J_4=(\rho+\mu)$, $J_5=(1-\theta)\rho$, $J_6=\delta+\gamma_1+\mu$, $J_7=\theta\rho$, $J_8=\delta+\gamma_2+\mu$, $J_9=(\alpha+\mu)$.
The characteristic polynomial equation of $J(\varepsilon_0^*,\beta_1^*)$ is obtained as

$$P(\lambda)=|J(\varepsilon_0^*,\beta_1^*)-\lambda I|=\lambda(\lambda+\mu)(\lambda+(\alpha+\mu))P_0(\lambda).$$

Where,

$$P_0(\lambda)=\lambda^3+B_1\lambda^2+B_2\lambda+B_3. \tag{15}$$

With,

$$\begin{cases} B_1=J_4+J_6+J_8+\mu_b, \\ B_2=J_4\mu_b+J_6\mu_b+J_8\mu_b+J_4J_6+J_4J_8+J_6J_8-J_1J_5-J_2J_7, \\ B_3=J_4J_6J_8+J_4J_6\mu_b+J_4J_8\mu_b+J_6J_8\mu_b-J_1J_5J_8-J_2J_6J_7-J_1J_5\mu_b-J_2J_7\mu_b-J_3J_5\eta-J_3J_7\eta. \end{cases}$$

Obviously, $\lambda_1=0,\lambda_2=-\mu,\lambda_3=-\alpha-\mu$ are the three eigenvalues of $J(\varepsilon_0^*,\beta_1^*)$. The other eigenvalues are the roots the polynomial $P_0(\lambda)$. Based on the Routh's criterion in Theorem 5.1 by (Martcheva, 2015), for the roots of the polynomial $P_0(\lambda)$ in (15) to have negative real parts the following conditions must be satisfied: $B_1>0, B_2>0, B_3>0$ and $B_1B_2-B_3>0$. Clearly, the first condition, $B_1=J_4+J_6+J_8+\mu_b=(\delta+\gamma_1+\mu)+(\delta+\gamma_2+\mu)+(\rho+\mu)+\mu_b>0$.

Now, we need to show the remaining three conditions. After several algebraic manipulations for the parameters of the coefficients B_2, B_3, and of the expression $B_1B_2-B_3$, we found

$$B_2=Q_1+Q_2+Q_3>0,\ \text{if } R_0\le 1 \quad \text{where,}\quad Q_1=\mu_b(J_4+J_6+J_8)+J_6J_8>0,$$
$$Q_2=\frac{1}{\mu}\left(\mu J_4J_6-\beta_2\Pi\sigma J_5\right)>0 \text{ if } R_0\le 1,\quad Q_3=\frac{1}{\mu}\left(\mu J_4J_8-\beta_2\Pi J_7\right)>0 \text{ if } R_0\le 1.$$
$$B_3=P_1+P_2+P_3+P_4>0,\ \text{for } R_0\le 1,\quad \text{where,}\quad P_1=J_6J_8\mu_b>0,$$
$$P_2=\frac{1}{C\mu_b}\left(C\mu_b\mu J_4J_6-\Pi J_5(C\mu_b\sigma\beta_2+\beta_1\eta)\right) \text{ if } R_0\le 1,$$
$$P_3=\frac{1}{C\mu_b}\left(C\mu_b\mu J_4J_8-\Pi J_7(C\mu_b\sigma\beta_2+\beta_1\eta)\right) \text{ for } R_0\le 1,$$
$$P_4=\frac{1}{\mu}\left(\mu J_4J_6J_8-\beta_2\Pi\rho(\theta J_6+\sigma(1-\theta)J_8)\right) \text{ for } R_0\le 1.$$
$$B_1B_2-B_3=A_2(J_5+\mu_b)+J_6^2(J_8+\mu_b)+J_8(J_6\mu_b+J_8\mu_b+J_4J_6+J_6J_8)$$
$$+\mu_b(J_1J_5+J_2J_7)+J_3\eta(J_5+J_7)+J_6Q_2+J_8Q_3>0 \ \text{ if } R_0\le 1.$$

Consequently, zero is a simple eigenvalue of $J(\varepsilon_0^*,\beta_1^*)$ and all other eigenvalues of $J(\varepsilon_0^*,\beta_1^*)$ have negative real numbers or real parts. Therefore, the center manifold theory (Carr, 2012) can be used to study the dynamics of (14) near β_1^*. Furthermore, it can be computed that $J(\varepsilon_0^*,\beta_1^*)$ has a right eigenvector corresponding to zero eigenvalue, given by $\mathbf{U}=\left(u_1,u_2,u_3,u_4,u_5,u_6\right)^T$, where

$$u_1=-\frac{u_2}{(\rho+\alpha)\mu J_6J_8}\left(\alpha\rho\gamma_2(\delta+\mu)(1-\theta)+\rho\alpha\gamma_1\theta+\rho\alpha(\delta+\mu)^2+\rho\mu J_6J_8+\mu(\alpha J_6J_8+\mu J_6J_8)\right)<0,$$
$$u_2=u_2>0,\quad u_3=u_2\frac{(1-\theta)\rho}{J_6},\quad u_4=u_2\frac{\theta\rho}{J_8},$$
$$u_5=u_2\left(\frac{\gamma_1\rho(1-\theta)J_8+\gamma_2\rho\theta J_6)}{(\alpha+\mu)J_6J_8}\right),\quad u_6=u_2\frac{\eta\rho(\theta J_6+(1-\theta)J_8)}{\mu_bJ_6J_8}.$$

Where, $J_6=\delta+\gamma_1+\mu, J_8=\delta+\gamma_2+\mu$.
Likewise, $J(\varepsilon_0^*,\beta_1^*)$ has a left eigenvector, $\mathbf{V}=\left(v_1,v_2,v_3,v_4,v_5,v_6\right)^T$ associated with $\lambda=0$, satisfying the condition $\mathbf{U}\,.\mathbf{V}=1$, with

$$v_1=0,\ v_2=v_2>0,\ v_3=v_2\frac{\Pi(\beta_2\sigma\mu_b\mathbf{C}+\beta_1^*\eta)}{\mathbf{C}\mu_b\mu J_6},\ v_4=v_2\frac{\Pi(\beta_2\mu_b\mathbf{C}+\beta_1^*\eta)}{\mathbf{C}\mu_b\mu J_8},\ v_5=0,\ v_6=v_2\frac{\beta_1^*\Pi}{\mathbf{C}\mu_b\mu}.$$

Computations of a and b: The local stability of ε_1^* for $R_0>1$, but near to the unity is determined by the signs of two associated constants a and b, where

$$a=\sum_{k,i,j=1}^{n} v_ku_iu_j\frac{\partial^2 f_k}{\partial x_i\partial x_j}(\varepsilon_0^*,\beta_1^*).$$
$$b=\sum_{k,i=1}^{n} v_ku_i\frac{\partial^2 f_k}{\partial x_i\beta_1^*}(\varepsilon_0^*,\beta_1^*).$$

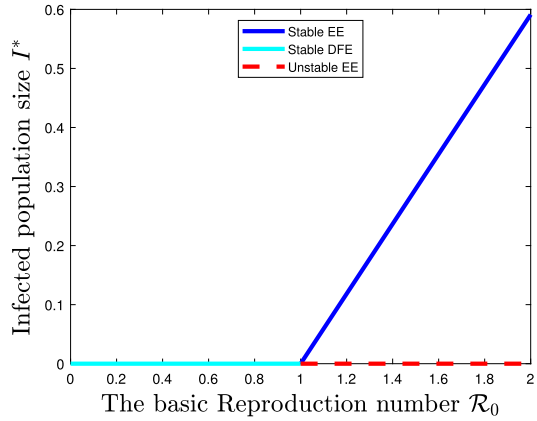

Fig. 2. Forward bifurcation plot for melioidosis model (2) using parameter values in Table 3.

Since $R_0 = 1$, $v_2 > 0$, $1 - \theta > 0$, and all parameters are positive. After some algebraic manipulations, we obtained:

$$a = -v_2 u_2^2 \left(\phi \frac{(\rho+\mu)\mu}{\Pi} + 2\left(\frac{\eta\rho\left[\theta(\delta+\gamma_1+\mu)+(1-\theta)(\delta+\gamma_2+\mu)\right]}{\mu_b \mathbf{C}(\delta+\gamma_1+\mu)(\delta+\gamma_2+\mu)} \right)^2 \frac{\beta_1 \Pi}{\mu} \right) < 0, \text{ (always)}$$

where,

$$\phi = \frac{\left(\alpha\rho\gamma_2(\delta+\mu)(1-\theta) + \rho\alpha\gamma_1\theta + \rho\alpha(\delta+\mu)^2 + \rho\mu J_6 J_8 + \mu(\alpha J_6 J_8 + \mu J_6 J_8)\right)}{(\rho+\alpha)\mu J_6 J_8} > 0,$$

and,

$$b = v_2 u_6 \frac{\partial^2 f_2}{\partial x_6 \partial \beta_1^*}(\epsilon_0^*, \beta_1^*) = v_2 u_2 \left(\frac{\Pi\eta\rho\left[\theta(\delta+\gamma_1+\mu)+(1-\theta)(\delta+\gamma_2+\mu)\right]}{\mu\mu_b \mathbf{C}(\delta+\gamma_1+\mu)(\delta+\gamma_2+\mu)} \right) > 0. \text{ (always)}$$

Based on the computed value of a and b, and with the help of Theorem 4.1 by Chavez and Song in (Castillo-Chavez and Song, 2004), the model exhibits a forward bifurcation at $R_0 = 1$ (see Fig. 2), and hence, the EE is locally asymptotically stable for $R_0 > 1$, but close to 1. The biological consequence of this is that the melioidosis disease can be eliminated from a community as long as if $R_0 < 1$. This completes the proof.

4. Sensitivity analysis

The sensitivity analysis for the basic reproduction number, R_0, of the melioidosis model parameters is performed following the approach in (Chitnis et al., 2008; Rosa and Torres, 2018; Aldila and Angelina, 2021; Purwati et al., 2020; Engida et al., 2022). This helps us to identify the parameters with a high impact on R_0 and also helps in providing appropriate intervention strategies. To measure the sensitivity of R_0 with respect to the model parameters we use a normalized forward sensitivity index of R_0, which is defined as the ratio of the relative change in the R_0 to the relative change in the parameter.

Definition 4.1. The normalized forward sensitivity index of the basic reproduction number, R_0, of the model (2), which is differentiable with respect to a given parameter α, is given by the relation

$$Y_\alpha^{R_0} = \frac{\partial R_0}{\partial \alpha} \times \frac{\alpha}{R_0}. \tag{16}$$

Therefore, using the equation (16) in the above Definition 4.1, we can easily derive an analytical expression for the sensitivity index of R_0, using the explicit formula (7), to each parameter that it includes.

Let $\phi_0 = \Pi\rho(\beta_1\eta(\theta\epsilon_1 + (1-\theta)\epsilon_2) + C\mu_b\beta_2(\theta\epsilon_1 + \sigma(1-\theta)\epsilon_2)$, $\phi_1 = (\rho+\mu)C\mu\mu_b\epsilon_1\epsilon_2$, $\epsilon_1 = \delta + \gamma_1 + \mu$, and $\epsilon_2 = \delta + \gamma_2 + \mu$. Thus,

$$\begin{aligned}
&Y_{\beta_1}^{R_0} = \frac{\beta_1\Pi\rho\eta\left(\theta\epsilon_1 + (1-\theta)\epsilon_2\right)}{\phi_0}, \quad Y_{\beta_2}^{R_0} = \frac{C\mu_b\beta_2\Pi\rho(\theta\epsilon_1 + \sigma(1-\theta)\epsilon_2)}{\phi_0}, \quad Y_\Pi^{R_0} = 1, \quad Y_\rho^{R_0} = \frac{\mu}{(\rho+\mu)},\\
&Y_\sigma^{R_0} = \frac{\beta_2\Pi\rho\sigma(1-\theta)}{\phi_0}, \quad Y_{\mathbf{C}}^{R_0} = -\frac{\beta_1\Pi\rho\eta(\theta\epsilon_1 + (1-\theta)\epsilon_2)}{\phi_0}, \quad Y_{\mu_b}^{R_0} = -\frac{\beta_1\Pi\rho\eta(\theta\epsilon_1 + (1-\theta)\epsilon_2)}{\phi_0},\\
&Y_\theta^{R_0} = \frac{\Pi\rho\theta\left[\beta_1\eta(\gamma_1-\gamma_2) + C\mu_b\beta_2(\gamma_1 - \sigma\gamma_2)\right]}{\phi_0}, \quad Y_\eta^{R_0} = \frac{\beta_1\Pi\rho\eta(\theta\epsilon_1 + (1-\theta)\epsilon_2)}{\phi_0},\\
&Y_\mu^{R_0} = \frac{\Pi\rho\mu\phi_1\left[\beta_1\eta + C\mu_b\beta_2(\theta + \sigma(1-\theta)\right] - \mu C\mu_b\phi_0\left((\rho+2\mu)\epsilon_1\epsilon_2 + (\rho+\mu)\mu(\epsilon_1+\epsilon_2)\right)}{\phi_0\phi_1},\\
&Y_\delta^{R_0} = \frac{\delta\epsilon_1\epsilon_2\Pi\rho\left[\beta_1\eta + C\mu_b\beta_2(\theta + \sigma(1-\theta))\right] - \phi_0\delta(\epsilon_1+\epsilon_2)}{\phi_0\epsilon_1\epsilon_2},
\end{aligned} \tag{17}$$

Table 3. Sensitivity indices of R_0 to the model parameter values.

Parameter	Value	Sensitivity index	Source
Π	$\mu \times N0$	1	(Terefe and Kassa, 2020)
β_2	0.00077	0.9437	Assumed
μ	0.000396	−1.0089	(Tavaen and Viriyapong, 2019)
θ	0.5125	0.2238	Assumed
δ	0.0732	−0.8148	(Terefe and Kassa, 2020)
γ_2	0.0157	−0.1498	(Mahikul et al., 2019)
β_1	0.0183	0.0563	Assumed
μ_b	0.0185	−0.0563	(Tavaen and Viriyapong, 2019)
C	5000	−0.0563	Assumed
η	0.13	0.0563	(Tavaen and Viriyapong, 2019)
σ	0.0493	0.0047	Assumed
γ_1	0.0248	−0.0147	(Mahikul et al., 2019)
ρ	0.088	0.0045	(Tavaen and Viriyapong, 2019)

Table 4. Values and description of parameters of the model.

Parameter	Description	Value	Unit	Source
Π	Human recruitment rate	$\mu \times N0$	Humans day^{-1}	(Terefe and Kassa, 2020)
β_1	Human transmission rate due to pathogen	0.0183	Day^{-1}	Assumed
β_2	Human transmission rate due to A & I	0.00077	(Humans day)$^{-1}$	Assumed
θ	Probability of progress of E to I	0.5125	Dimensionless	Assumed
μ	Natural death rate of humans	0.000396	Day^{-1}	(Tavaen and Viriyapong, 2019)
δ	Disease-induced death rate of A & I	0.0732	Day^{-1}	(Terefe and Kassa, 2020)
γ_1	Recovery rate from A	0.0248	Day^{-1}	(Mahikul et al., 2019)
γ_2	Recovery rate from I	0.0157	Day^{-1}	(Mahikul et al., 2019)
ρ	The progression rate of E to A & I	0.088	Day^{-1}	(Tavaen and Viriyapong, 2019)
σ	Reduction rate of infectivity A	0.0493	Dimensionless	Assumed
α	Disease waning immunity	0.0726	Day^{-1}	Assumed
η	Rate at which bacteria increase by A & I	0.13	$\frac{\text{No. of } B.\ pseudomallei \text{ cell}}{\text{Humans day}}$	(Tavaen and Viriyapong, 2019)
μ_b	Natural death rate of bacteria	0.0185	Day^{-1}	(Tavaen and Viriyapong, 2019)
C	Concentration of *B. pseudomallei*	5000	No. of *B. pseudomallei* cell	Assumed

$$Y_{\gamma_1}^{R_0} = \frac{\epsilon_1\gamma_1\left[\Pi\rho\beta_1\eta\left(\theta+(1-\theta)\epsilon_2\right)+C\mu_b\beta_2\Pi\rho\left(\theta+\sigma(1-\theta)\epsilon_2\right)\right]-\phi_0\gamma_1}{\phi_0\epsilon_1},$$

$$Y_{\gamma_2}^{R_0} = \frac{\epsilon_2\gamma_2\left[\Pi\rho\beta_1\eta\left(\theta\epsilon_1+(1-\theta)\right)+C\mu_b\beta_2\Pi\rho\left(\theta\epsilon_1+\sigma(1-\theta)\right)\right]-\phi_0\gamma_2}{\phi_0\epsilon_2}.$$

In particular, the sensitivity index of R_0 related to the recruitment rate, Π, is found in (17) using (16) as $Y_{\Pi}^{R_0} = \frac{\partial R_0}{\partial \Pi} \times \frac{\Pi}{R_0} = 1$.

Similarly, the detailed sensitivity indices of R_0 to the parameter values are described in Table 3 from the most sensitive parameter to the least sensitive parameter. In Table 3, the positive sign of $Y_{\alpha}^{R_0}$ shows a positive impact of the parameter α on R_0 (directly proportional). Whereas the negative sign of $Y_{\alpha}^{R_0}$ shows a negative impact of α on R_0 (indirectly proportional). For instance, decreasing β_2 by 10% results in a decrease R_0 by 9.44%. Similarly, increasing (or decreasing) β_2 by 15% results in an increase (or decrease, respectively) the value of R_0 by 14.16%. This suggests that preventive measures should be provided to reduce the spread of the disease. In contrast, increasing γ_2 by 10% results in decreases R_0 by 1.67%. Likewise, increasing μ_b by 10% would decrease R_0 by 0.56%. This means that increasing the mortality rate of the *Burkholderia pseudomallei* in the environment by using an appropriate intervention effort would decrease the spread of disease. The results in the Table 3 show that decreasing the value of the parameters $\Pi, \beta_1, \beta_2, \theta, \eta, \rho, \sigma$ would decrease the value of R_0. Conversely, R_0 decreases when the parameters $\delta, \mu, \mu_b, \gamma_1, \gamma_2, \mathbf{C}$ increase.

In view of the results of the sensitivity analysis, the most influencing parameters are human recruitment rate (Π), human transmission rate (β_2), the human natural death rate (μ), and disease-induced death rate (δ) among other parameters. This demonstrates that melioidosis spread can be controlled by reducing the human transmission rate, β_2, on susceptible humans. As a result, preventive intervention efforts should be provided to combat the burden of the disease in the population. Moreover, when the value of reduction rate of A (σ) is 0.5, then the value of R_0 will increase by 35.22% and if the value of σ is 1, the value of will increase by 74.28%. Therefore, although the asymptomatic infections are difficult to diagnose they have a great impact on the spread of the disease in the population. Also, it has a great role in increasing the growth of *Burkholderia pseudomallei* in the environment.

5. Numerical results and discussions

The model (2) is numerically simulated to show the effect of the most influencing parameters on disease dynamics. To accomplish this, the fourth-order Runge-Kutta method is applied in the Matlab. The parameter values used for simulations are described in Table 4 and the initial conditions are considered as $(S_0, E_0, A_0, I_0, R_0, B_{m0}) = (700, 20, 0, 10, 0, 300)$. We used these parameter values and the initial conditions in all simulations of the model. In Figs. 3 and 4, it is noted that all model solution trajectories ultimately remain in the positively invariant region Ω_m whenever the initial values are in Ω_m. The basic reproduction number of the model (2) is obtained as $R_0 \approx 3.5482 > 1$. From the equation (15), we found the unique positive endemic equilibrium, $\varepsilon_1^* = \left(205.7844, 2.976, 1.2975, 1.503, 0.7641, 19.6794\right)$ for $I^* \approx 1.503$, which is locally asymptotically stable for $R_0 > 1$ and the others are negative (unstable). As a result, all model solution trajectories move towards the steady-state ε_1^* as demonstrated in Figs. 3 (a) - 3 (e). In addition, the graphs show that the number of infected classes endures in population and that each one gradually goes to the small positive constant (to the corresponding component of ε_1^*). However, if we modify the values of $\beta_1, \beta_2, \gamma_1$ and γ_2 into $0.015, 0.00027, 0.058$ and 0.0527, respectively, it gives $R_0 \approx 0.951 < 1$. Thus, ε_1^* is unstable since the model in this case contains a DFE that is globally asymptotically stable. As a result,

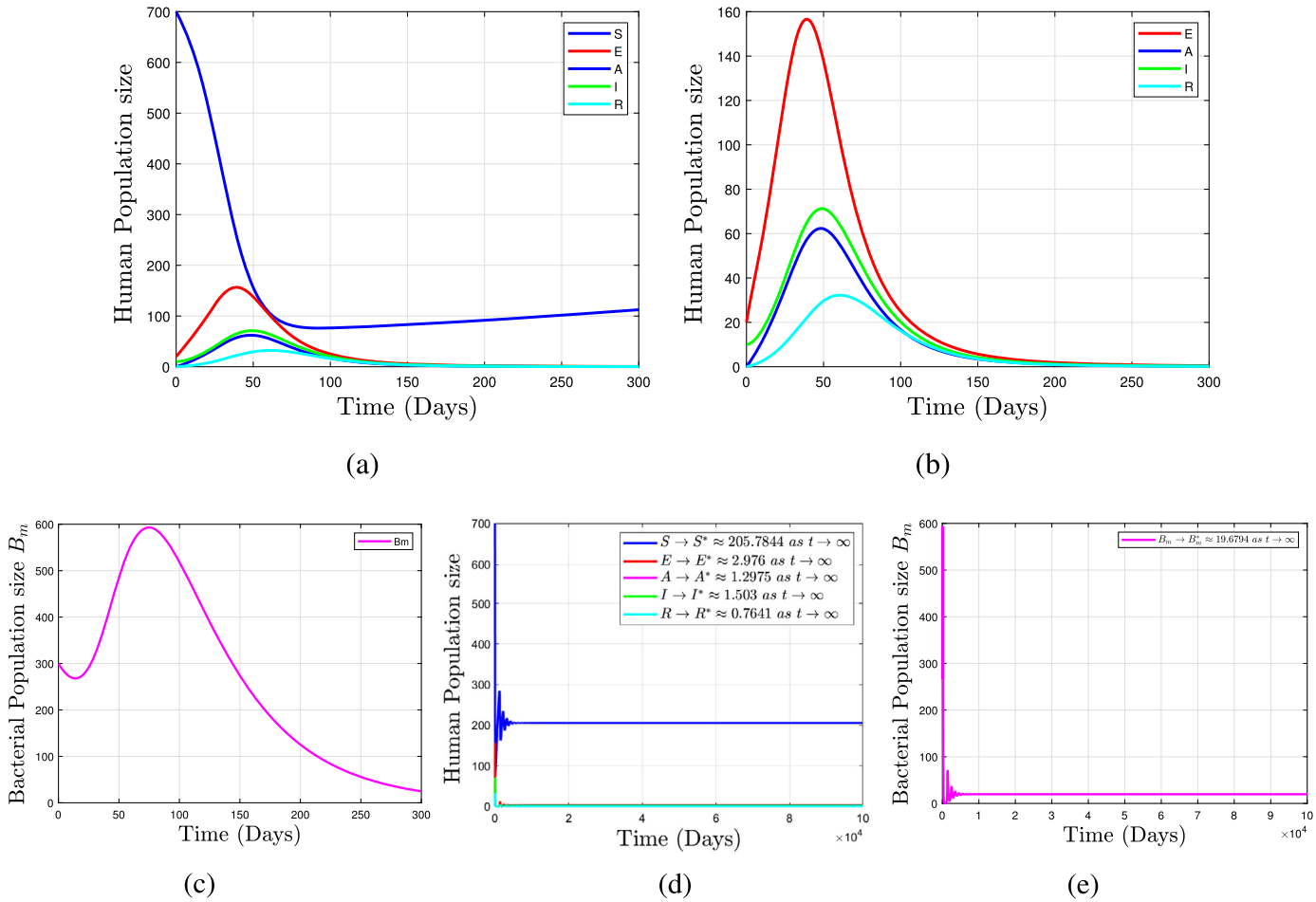

Fig. 3. Simulations illustrating the asymptomatic stability of the endemic equilibrium (ε_1^*) of the system (2) for $R_0 > 1$. (a) The stability behavior of the human population components of (ε_1^*) over the simulation period, (b) The stability behavior of the infected and recovered individual components of (ε_1^*) over the simulation period, (c) The stability behavior of the bacterial population component of (ε_1^*) over the simulation period, (d) The stability behavior of the human population components of (ε_1^*) as t gets large and (e) The stability behavior of the bacterial population component of (ε_1^*) as t gets large.

all model solution trajectories move to DFE over time as depicted in Figs. 4 (a) - 4 (e). Biologically implication is that the disease will die out from the community over time, while the trajectory of susceptible humans eventually tends to $\frac{\Pi}{\mu} = 730$ for this particular study. Therefore, in order to eliminate the disease rapidly, we should lower the value of R_0 as much as we can.

5.1. Impacts of the parameters $\beta_1 \& \beta_2$ on transmission process of the disease

In this section, we demonstrate the effects of the parameters β_1 and β_2 on the dynamics of melioidosis transmission by varying their values. These parameters significantly contribute to the spread of the disease by enhancing the force of infection in the transmission process of the epidemic. From Fig. 6 (a), we observed that increasing the value of β_2 will significantly increase the number of susceptible individuals getting infected (or reduce the number of susceptible humans). In other words, the number of susceptible individuals is inversely proportional to β_2. However, decreasing this parameter's value will gradually decrease both the size of the bacterial population and the number of infectious humans (both symptomatic or asymptomatic) as confirmed in Figs. 6 (b) - 6 (d). In addition, reducing the value of β_2 reduces the value of R_0. As a result, the infectious classes could finally vanish by considerably lowering the value of β_2. This can be accomplished by providing appropriate personal preventive interventions for susceptible humans and by treating infectious classes. Similarly, in Figs. 5 (a) - 5 (c), we observed the impact of the transmission rate, β_1, on classes of susceptible, infectious and bacterial. Furthermore, from the findings of the impacts of the transmission rates, we conclude that reducing $\beta_1 \& \beta_2$ on susceptible humans is essential for minimizing the spread of disease infection.

5.2. Impact of the shedding rate of Burkholderia pseudomallei (η)

By releasing the organism into the environment, infectious individuals (both asymptomatic and symptomatic) contribute significantly to the growth of *B. pseudomallei*, which in turn increases the rate at which the disease spreads from the environment. Fig. 7 (a) and 7 (b), show the impacts of η on populations of susceptible individuals and bacterial, respectively. As illustrated in Fig. 7 (b), it is noted that increasing the value of η increases the size of the bacterial population dramatically. Whereas in Fig. 7 (a), the size of susceptible individuals increases as η diminishes over time. This demonstrates that in order to decrease the rate of shedding of the *B. pseudomallei*, a control intervention strategy (typically treatment control) should be applied to infectious individuals. As a result, there will be a decrease in the growth of *B. pseudomallei* in the environment. In other words, the number of susceptible individuals getting infected will be diminished.

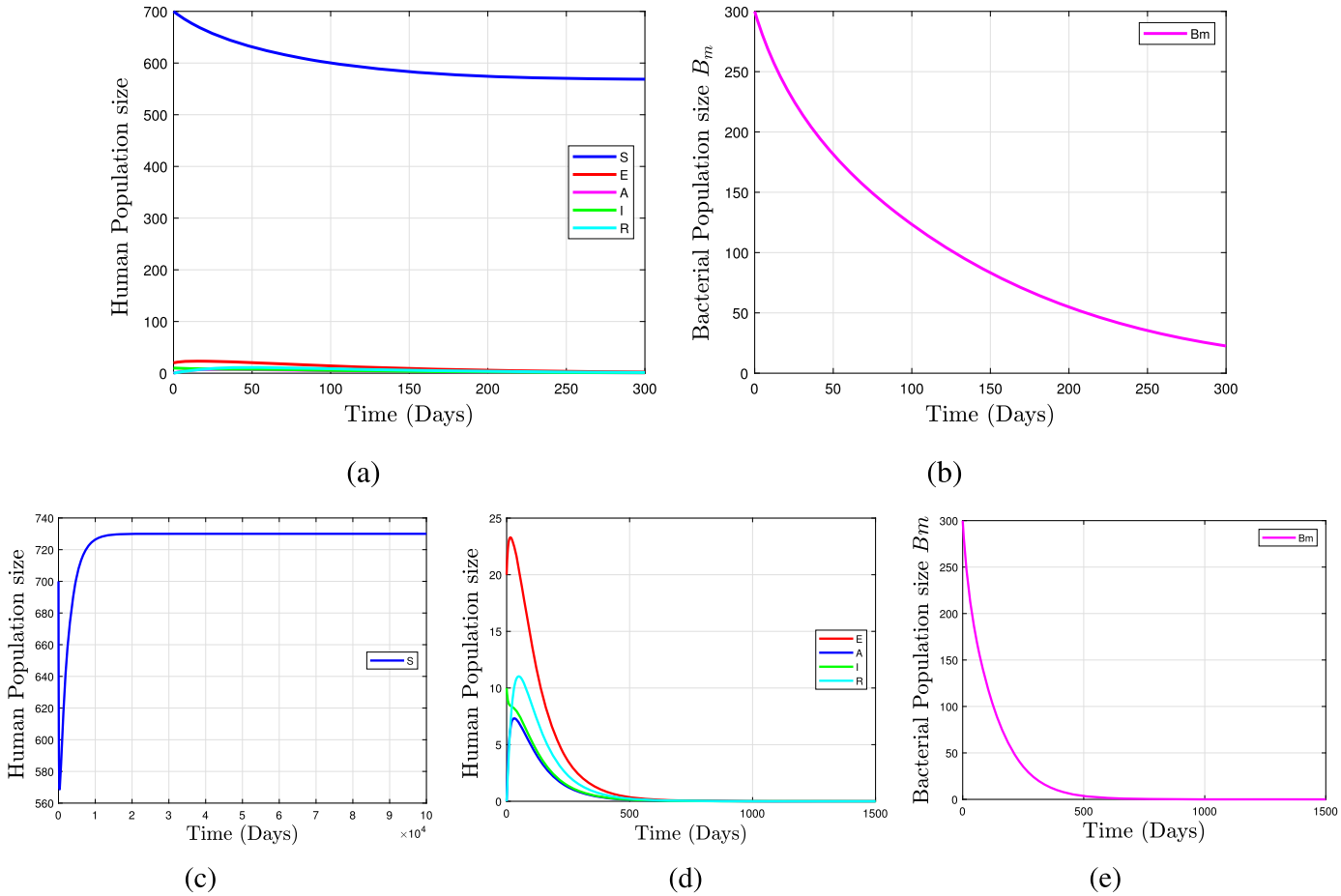

Fig. 4. Simulations illustrating the global asymptomatic stability of the DFE = $(730, 0, 0, 0, 0, 0)$ of the system (2) for $R_0 < 1$. (a) The stability behavior of the human population components of DFE over the simulation period, (b) The stability behavior of the bacterial population component of DFE over the simulation period, (c) The stability behavior of the susceptible human component of DFE as t gets large, (d) The stability behavior of the infected and recovered individual components of DFE as t gets large and (e) The stability behavior of the bacterial population component of DFE as t gets large.

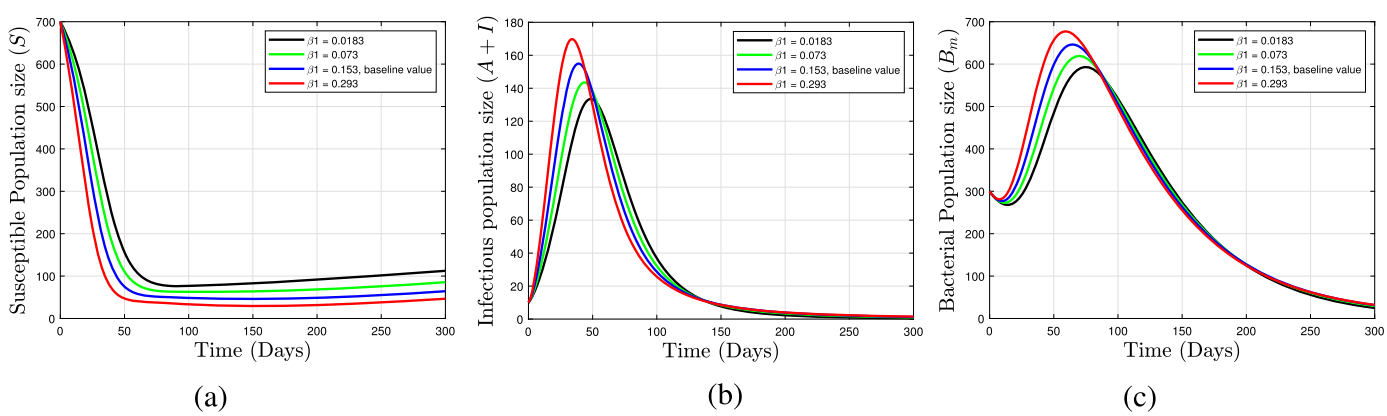

Fig. 5. Simulations illustrating the changing effect of β_1 on the model (2); (a) variation of susceptible individuals for different values of β_1, (b) variation of infectious individuals $(I + A)$ for different values of β_1 and (c) variation of bacterial population for different values of β_1.

5.3. Impacts of the recovery rates (γ_1&γ_2)

In Figs. 8 (a) & 8 (d), and in Figs. 9 (a) & 9 (e), we observed that the populations of susceptible and recovered humans decrease as recovery rates decrease. On the other hand, in Figs. 8 (b), 8 (c) & 8 (e), and Figs. 9 (b) - 9 (d) & 9 (f), we noted that the recovery rates are indirectly related to the number of infectious individuals (symptomatic and asymptomatic) and bacterial population. This shows that the number of infectious humans will be greatly diminished (or recovered humans will be increased) by providing the intervention control measure (treatment) in the population. However, the population of susceptible individuals increases as recovery rates increase because of the disease waning immunity as confirmed in Fig. 8 (a) and Fig. 9 (a). Thus, in addition, a preventive intervention strategy should be provided to diminish the disease spread.

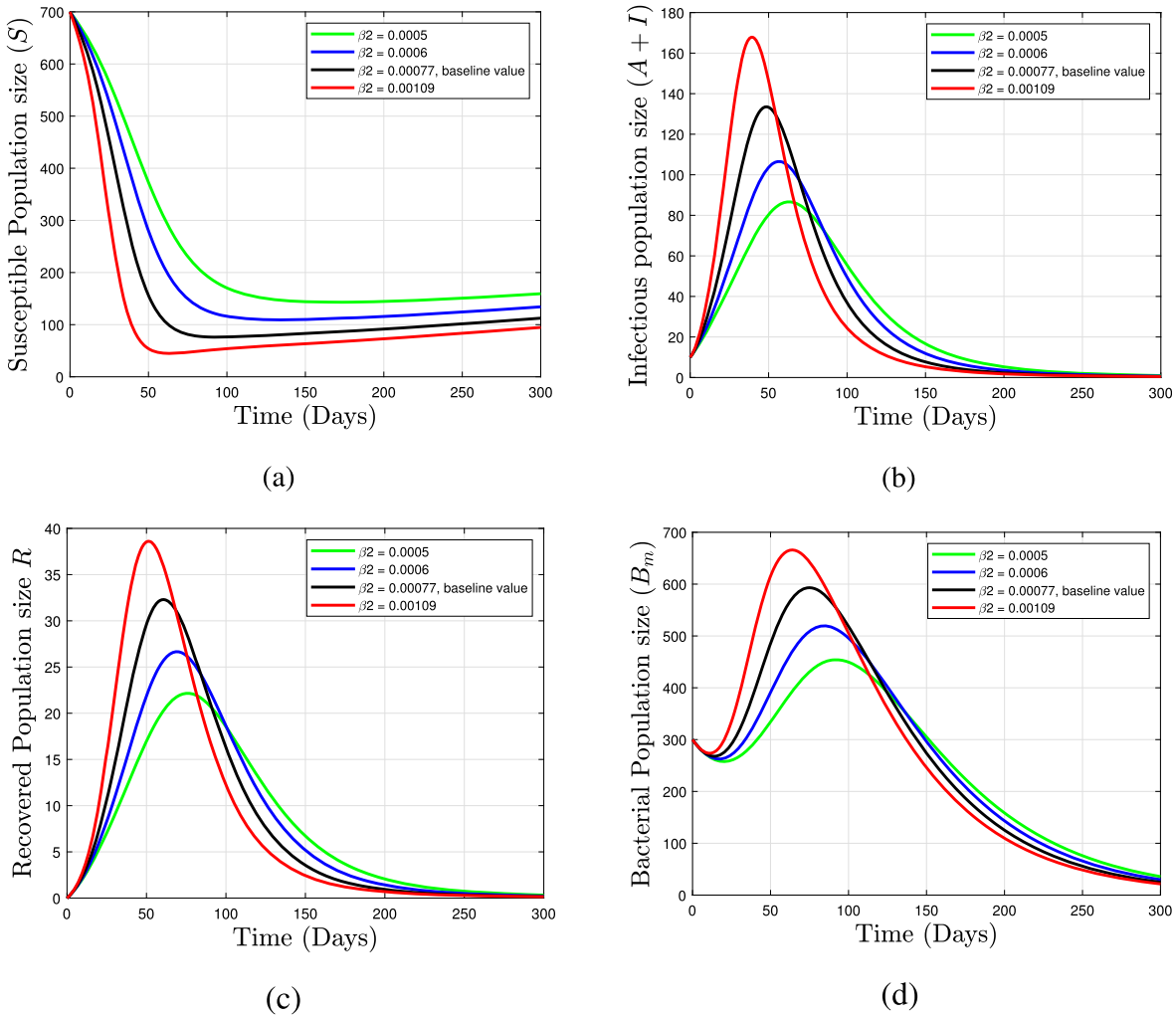

Fig. 6. Simulations illustrating the changing effect of β_2 on the model (2); (a) variation of susceptible individuals for different values of β_2, (b) variation of infectious individuals $(I + A)$ for different values of β_2, (c) variation of recovered individuals for different values of β_2 and (d) variation of bacterial population for different values of β_2.

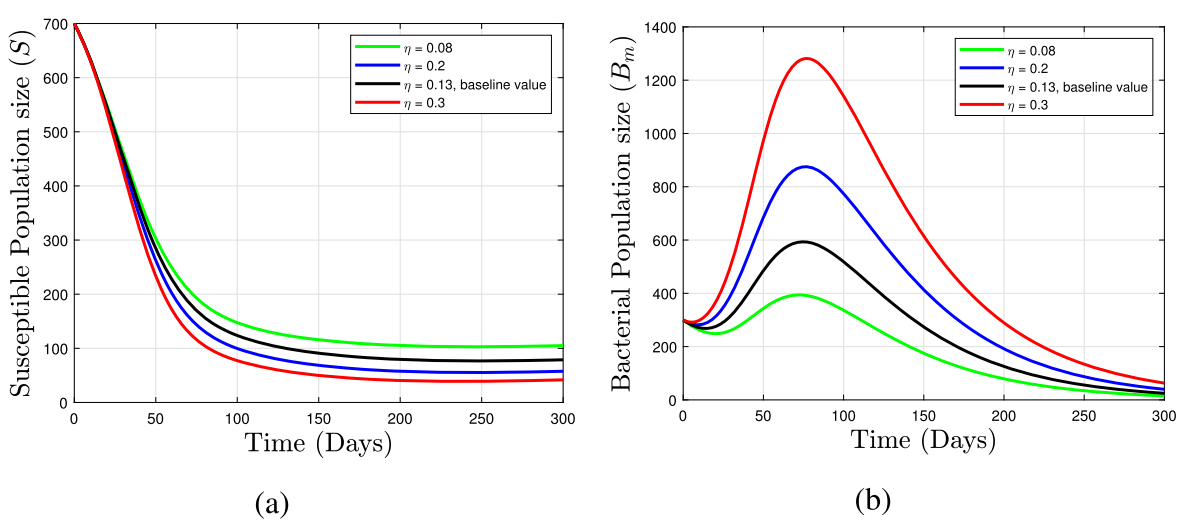

Fig. 7. Simulations illustrating the changing effect of η on the model (2); (a) variation of susceptible individuals for different values of η and (b) variation of bacterial population for different values of η.

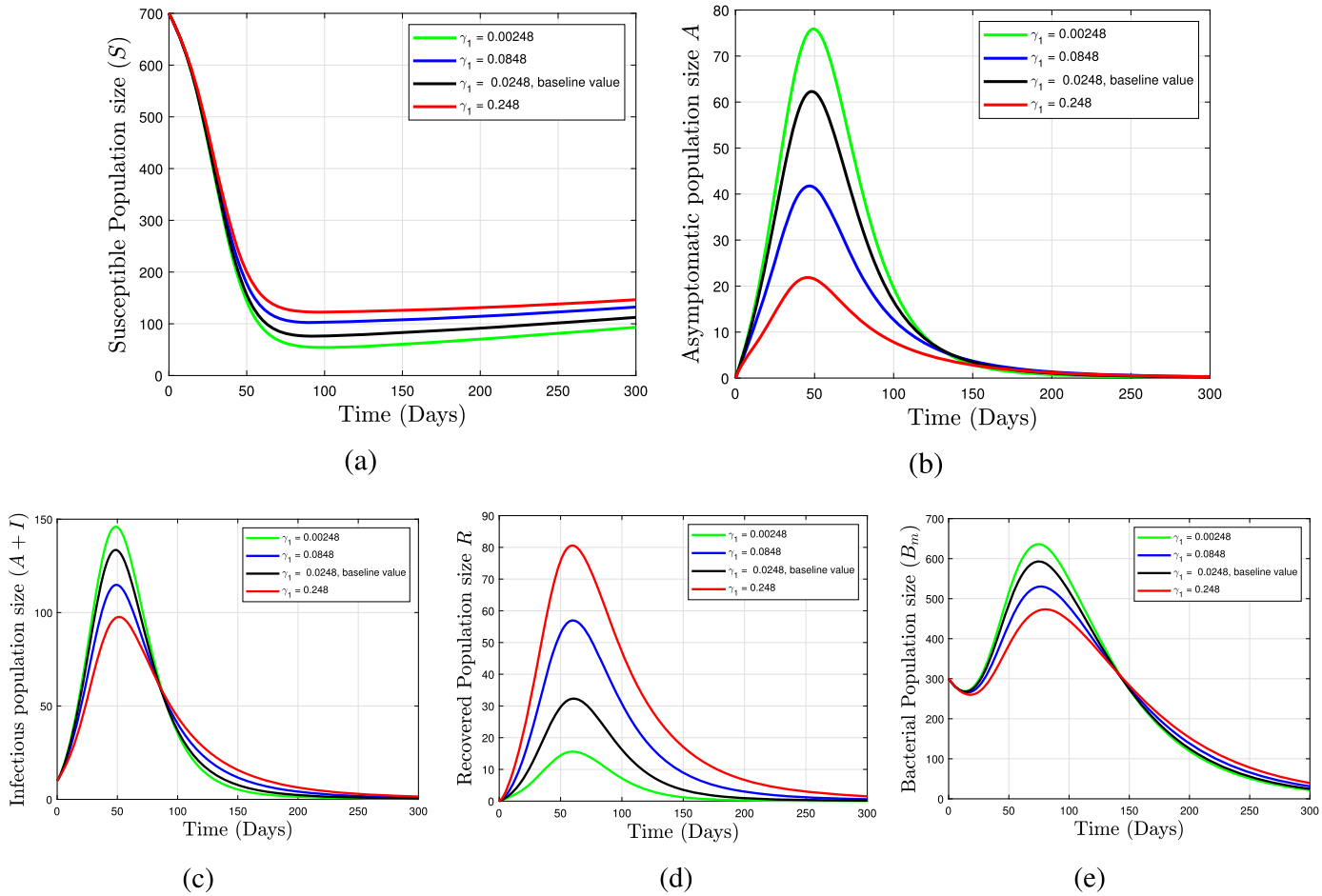

Fig. 8. Simulations illustrating the changing effect of γ_1 on the model (2); (a) variation of susceptible individuals for different values of γ_1, (b) variation of asymptomatic infectious individuals A for different values of γ_1, (c) variation of infectious individuals $(I + A)$ for different values of γ_1, (d) variation of recovered individuals for different values of γ_1 and (e) variation of bacterial population for different values of γ_1.

6. Conclusion

Transmission of disease infection in humans that usually occur due to interaction with a contaminated environment can be reduced by avoiding contact with the contaminated sources or using treated water for drinking, which, as in the case of melioidosis. In this paper, we proposed a compartmental model that explains the dynamics of melioidosis transmission with an asymptomatic class in the human population. The formulated model has a disease-free equilibrium (DFE), which is globally asymptotically stable (GAS) whenever the basic reproduction number (R_0) is less than unity. Whereas the endemic equilibrium of the model is shown to be locally asymptotically stable when R_0 is greater than unity. Sensitivity analysis results indicate that the recruitment rate (Π) is the most influential parameter followed by the transmission coefficient (β_2). Thus, the parameter β_2 plays an important role to minimize the spread of disease infection. Furthermore, the numerical simulations of the steady state deduced that every solution of the model approaches the unique positive endemic equilibrium, ε_1^*, over time for $R_0 \approx 3.5482 > 1$, as confirmed in Figs. 3 (a) - 3 (e). From numerical findings, we also noted that the populations of infectious individuals (both asymptomatic and symptomatic) and bacterial diminish when transmission rates decrease, see, Figs. 5 (a) - 5 (c) and Figs. 6 (b) - 6 (d). While these population groups increase as the recovery rates of infectious individuals decrease. In contrast, the number of susceptible individuals increases as the recovery rates increase due to the disease waning immunity (see Fig. 8 (a) and Fig. 9 (a)). Our study suggests that in order to minimize the spread of the disease in the population, treatment of both asymptomatic and symptomatic infected individuals needs to be scaled up and human transmission coefficients should be reduced.

Declarations

Author contribution statement

Habtamu Ayalew Engida: Conceived and designed the experiments; Performed the experiments; Analyzed and interpreted the data; Wrote the paper.

David Mwangi Theuri, Duncan Gathungu, John Gachohi: Contributed reagents, materials, analysis tools or data; Analyzed and interpreted the data.

Haileyesus Tessema Alemneh: Conceived and designed the experiments; Contributed reagents, materials, analysis tools or data.

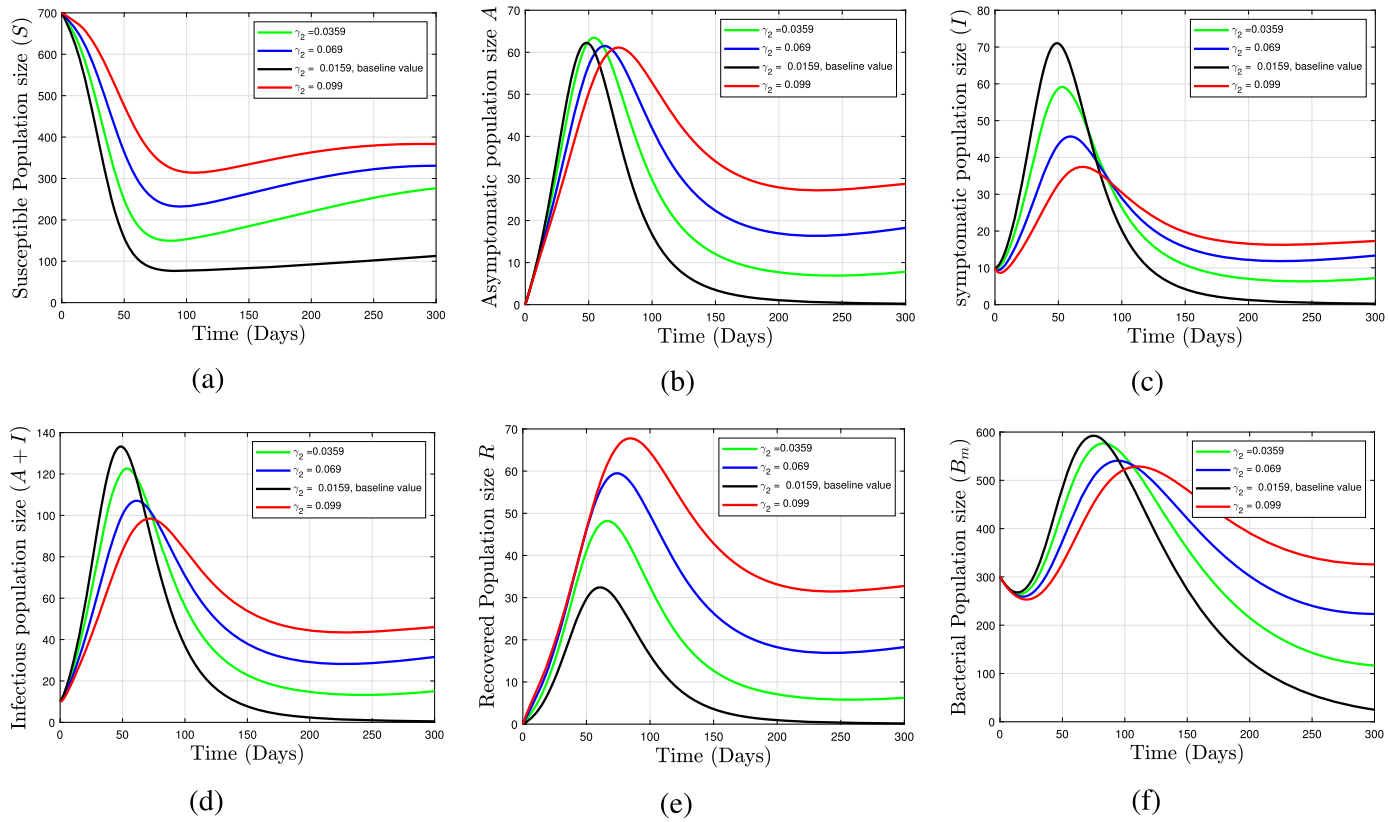

Fig. 9. Simulations illustrating the changing effect of γ_2 on the model (2); (a) variation of susceptible individuals for different values of γ_2, (b) variation of asymptomatic infectious individuals A for different values of γ_2, (c) variation of symptomatic infectious individuals I for different values of γ_2, (d) variation of infectious individuals $(I + A)$ for different values of γ_2, (e) variation of recovered individuals for different values of γ_2 and (f) variation of bacterial population for different values of γ_2.

Funding statement

This research did not receive any specific grant from funding agencies in the public, commercial, or not-for-profit sectors.

Data availability statement

Data included in article/supplementary material/referenced in article.

Declaration of interests statement

The authors declare no conflict of interest.

Additional information

No additional information is available for this paper.

Acknowledgements

The authors would like to thank Pan African University for providing the necessary support.

References

Aldila, D., Angelina, M., 2021. Optimal control problem and backward bifurcation on malaria transmission with vector bias. Heliyon 7 (4), e06824.
Benoit, T.J., Blaney, D.D., Gee, J.E., Elrod, M.G., Hoffmaster, A.R., Doker, T.J., Bower, W.A., Walke, H.T., 2015. Melioidosis cases and selected reports of occupational exposures to Burkholderia pseudomallei—United States, 2008–2013. Morb. Mortal. Wkly. Rep., Surveill. Summ. 64 (5), 1–9.
Carr, J., 2012. Applications of Centre Manifold Theory, vol. 35. Springer Science & Business Media.
Castillo-Chavez, C., Feng, Z., Huang, W., et al., 2002. On the computation of R_0 and its role in global stability. IMA Vol. Math. Appl. 125, 229–250.
Castillo-Chavez, C., Song, B., 2004. Dynamical models of tuberculosis and their applications. Math. Biosci. Eng. 1 (2), 361.
Chakravorty, A., Heath, C.H., 2019. Melioidosis: an updated review. Aust. J. Gen. Pract. 48 (5), 327–332.
Chitnis, N., Hyman, J.M., Cushing, J.M., 2008. Determining important parameters in the spread of malaria through the sensitivity analysis of a mathematical model. Bull. Math. Biol. 70 (5), 1272.
Chowdhury, S., Barai, L., Afroze, S.R., Ghosh, P.K., Afroz, F., Rahman, H., Ghosh, S., Hossain, M.B., Rahman, M.Z., Das, P., et al., 2022. The epidemiology of melioidosis and its association with diabetes mellitus: a systematic review and meta-analysis. Pathogens 11 (2), 149.

Currie, B.J., 2015. Melioidosis: evolving concepts in epidemiology, pathogenesis, and treatment. In: Seminars in Respiratory and Critical Care Medicine, vol. 36. Thieme Medical Publishers, pp. 111–125.
Currie, B.J., Kaestli, M., 2016. A global picture of melioidosis. Nature 529 (7586), 290–291.
Dutta, S., Haq, S., Hasan, M.R., Haq, J.A., 2017. Antimicrobial susceptibility pattern of clinical isolates of Burkholderia pseudomallei in Bangladesh. BMC Res. Notes 10 (1), 1–5.
Elbasha, E., Podder, C., Gumel, A., 2011. Analyzing the dynamics of an sirs vaccination model with waning natural and vaccine-induced immunity. Nonlinear Anal., Real World Appl. 12 (5), 2692–2705.
Engida, H.A., Theuri, D.M., Gathungu, D., Gachohi, J., Alemneh, H.T., 2022. A mathematical model analysis for the transmission dynamics of leptospirosis disease in human and rodent populations. Comput. Math. Methods Med.
Fen, S.H.Y., Tandhavanant, S., Phunpang, R., Ekchariyawat, P., Saiprom, N., Chewapreecha, C., Seng, R., Thiansukhon, E., Morakot, C., Sangsa, N., et al., 2021. Antibiotic susceptibility of clinical Burkholderia pseudomallei isolates in northeast Thailand during 2015-2018 and the genomic characterization of β-lactam-resistant isolates. Antimicrob. Agents Chemother.
Gumel, A.B., 2012. Causes of backward bifurcations in some epidemiological models. J. Math. Anal. Appl. 395 (1), 355–365.
Hinjoy, S., Hantrakun, V., Kongyu, S., Kaewrakmuk, J., Wangrangsimakul, T., Jitsuronk, S., Saengchun, W., Bhengsri, S., Akarachotpong, T., Thamthitiwat, S., et al., 2018. Melioidosis in Thailand: present and future. Trop. Med. Infect. Dis. 3 (2), 38.
Kanyi, E., Afolabi, A.S., Onyango, N.O., 2021. Mathematical modeling and analysis of transmission dynamics and control of schistosomiasis. J. Appl. Math. 2021.
Karunarathna, A., Mendis, S., Perera, W., Patabendige, G., Pallewatte, A., Kulatunga, A., 2018. A case report of melioidosis complicated by infective sacroiliitis in Sri Lanka. Trop. Dis. Travel Med. Vaccines 4 (1), 1–6.
Lakshmikantham, V., Leela, S., Martynyuk, A.A., 1989. Stability Analysis of Nonlinear Systems. Springer.
Levin, S.A., 2020. Descartes' rule of signs-how hard can it be?
Li, M.Y., 2018. An Introduction to Mathematical Modeling of Infectious Diseases, vol. 2. Springer.
Liao, S., Wang, J., 2011. Stability analysis and application of a mathematical cholera model. Math. Biosci. Eng. 8 (3).
Libotte, G.B., Lobato, F.S., Platt, G.M., Neto, A.J.S., 2020. Determination of an optimal control strategy for vaccine administration in covid-19 pandemic treatment. Comput. Methods Programs Biomed. 196, 105664.
Limmathurotsakul, D., Golding, N., Dance, D.A., Messina, J.P., Pigott, D.M., Moyes, C.L., Rolim, D.B., Bertherat, E., Day, N.P., Peacock, S.J., et al., 2016. Predicted global distribution of Burkholderia pseudomallei and burden of melioidosis. Nat. Microbiol. 1 (1), 1–5.
Luangasanatip, N., Flasche, S., Dance, D.A., Limmathurotsakul, D., Currie, B.J., Mukhopadhyay, C., Atkins, T., Titball, R., Jit, M., 2019. The global impact and cost-effectiveness of a melioidosis vaccine. BMC Med. 17 (1), 1–11.
Mahikul, W., White, L.J., Poovorawan, K., Soonthornworasiri, N., Sukontamarn, P., Chanthavilay, P., Medley, G.F., Pan-Ngum, W., 2019. Modelling population dynamics and seasonal movement to assess and predict the burden of melioidosis. PLoS Negl. Trop. Dis. 13 (5), e0007380.
Martcheva, M., 2015. An Introduction to Mathematical Epidemiology, vol. 61. Springer.
Phillips, N., Cervin, A., Earnshaw, J., Sidjabat, H., 2016. Melioidosis in a patient with chronic rhinosinusitis. J. Laryngol. Otol. 130 (S4), S60–S62.
Purwati, U.D., Riyudha, F., Tasman, H., et al., 2020. Optimal control of a discrete age-structured model for tuberculosis transmission. Heliyon 6 (1), e03030.
Rosa, S., Torres, D.F., 2018. Parameter estimation, sensitivity analysis and optimal control of a periodic epidemic model with application to hrsv in Florida. arXiv preprint, arXiv: 1801.09634.
Ross, B.N., Myers, J.N., Muruato, L.A., Tapia, D., Torres, A.G., 2018. Evaluating new compounds to treat Burkholderia pseudomallei infections. Front. Cell. Infect. Microbiol. 8, 210.
Saechan, V., Tongthainan, D., Fungfuang, W., Tulayakul, P., Ieamsaard, G., Ngasaman, R., 2022. Natural infection of leptospirosis and melioidosis in long-tailed macaques (Macaca fascicularis) in Thailand. J. Vet. Med. Sci. 84 (5), 700–706.
Sengyee, S., Saiprom, N., Paksanont, S., Limmathurotsakul, D., Wuthiekanun, V., Chantratita, N., 2017. Susceptibility of clinical isolates of Burkholderia pseudomallei to a lipid a biosynthesis inhibitor. Am. J. Trop. Med. Hyg. 97 (1), 62.
Singh, M., Mahmood, M., 2017. Melioidosis: the great mimicker. J. Community Hosp. Intern. Med. Perspect. 7 (4), 245–247.
Sullivan, R.P., Marshall, C.S., Anstey, N.M., Ward, L., Currie, B.J., 2020. 2020 review and revision of the 2015 Darwin melioidosis treatment guideline; paradigm drift not shift. PLoS Negl. Trop. Dis. 14 (9), e0008659.
Tauran, P.M., Sennang, N., Rusli, B., Wiersinga, W.J., Dance, D., Arif, M., Limmathurotsakul, D., 2015. Emergence of melioidosis in Indonesia. Am. J. Trop. Med. Hyg. 93 (6), 1160–1163.
Tavaen, S., Viriyapong, R., 2019. Global stability and optimal control of melioidosis transmission model with hygiene care and treatment. Int. J. Sci. 16 (2), 31–48.
Terefe, Y.A., Kassa, S.M., 2020. Analysis of a mathematical model for the transmission dynamics of human melioidosis. Int. J. Biomath. 13 (07), 2050062.
Van den Driessche, P., Watmough, J., 2002. Reproduction numbers and sub-threshold endemic equilibria for compartmental models of disease transmission. Math. Biosci. 180 (1–2), 29–48.
Wiersinga, W.J., Virk, H.S., Torres, A.G., Currie, B.J., Peacock, S.J., Dance, D.A., Limmathurotsakul, D., 2018. Melioidosis. Nat. Rev. Dis. Primers 4 (1), 1–22.